Waterspout Velocity Measurements by Airborne Doppler Lidar

R. L. SCHWIESOW AND R. E. CUPP

National Oceanic and Atmospheric Administration, Wave Propagation Laboratory, Boulder, Colorado 80303

P. C. SINCLAIR

Colorado State University, Atmospheric Science Department, Ft. Collins 80521

R. F. ABBEY, JR.

U.S. Nuclear Regulatory Commission, Office of Nuclear Regulatory Research, Washington, D.C. 20555

(Manuscript received 12 August 1980, in final form 20 December 1980)

ABSTRACT

A Doppler lidar measures the line-of-sight velocity of cloud droplets in a waterspout much as a meteorological Doppler radar measures the velocity of larger hydrometeors. We discuss details of the application of an airborne Doppler lidar to waterspout velocity measurements, including intensity weighting and limitations of the technique. One type of result available from the lidar data is the velocity spectrum of the line-of-sight velocity component of scatterers in the flow, integrated along the lidar axis, as a function of distance from the vortex axis. From the velocity spectra, peak winds in the portion of the waterspout marked by cloud droplets, turbulence levels, and interaction with the ambient flow can be inferred. In one example the maximum velocity observed in the visible part of the waterspout is 10 m s^{-1}. This double-walled waterspout showed a two-peaked velocity spectrum, which we interpret as a dynamic difference between the two coaxial components of the vortex.

1. Objective and background of the research

The purpose of this study was to apply airborne Doppler lidar techniques to the measurement of wind speeds in waterspouts. The emphasis here is on the instrumentation and the types of waterspout data available from the lidar. A subsequent paper will treat the total data set as it applied to waterspout structure.

Several features of lidar velocity instrumentation were useful for this application. The lidar can be located a few hundred meters away from the waterspouts (depending on system parameters), avoiding the necessity of close approach or an accurately known distance from the vortex as in the case of aircraft penetration, instrument pod penetration, or photogrammetry. There is no flow disturbance near the vortex core from the probe or aircraft platform. The line-of-sight velocity component of scattering particles (cloud droplets in this case) is known directly, without need for experimental calibration.

Waterspout velocity measurements are important in developing an understanding of the dynamics of waterspouts. Waterspouts are qualitatively similar to tornadoes but are easier to study because they are less violent and occur frequently in some areas. Information on the waterspout flow field may lead to a model that permits insight into the tornado-waterspout relationship. Data on peak winds and turbulence may also help in the design of facilities, such as hospitals and dockage, that are located in areas where waterspouts occur.

Previous work relevant to our study includes research by Golden (1974), who used photogrammetry to obtain remote measurements of waterspout velocities. Because the Doppler lidar method measures the line-of-sight velocity components (longitudinal) of an array or distribution of scatterers, it is partially complementary to photogrammetric instrumentation, which measures transverse velocity components (perpendicular to the line-of-sight) by tracking moving cloud tags. Other work on instrumentation for waterspout velocity data has used *in situ* probes rather than the remote sensing techniques of Doppler lidar and photogrammetry. Church *et al.*[1] attempted measurements with airplane-towed instrument packages swung into the vortex, and Leverson *et al.* (1977) made direct aircraft penetrations. An application of continuous-wave radar to the tor-

[1] Church, C. R., C. M. Ehresman and J. H. Golden, 1973: Instrumentation for probing waterspouts. *Preprints Seventh Conf. Severe Local Storms*, Kansas City, Amer. Meteor. Soc., 277–283.

0021-8952/81/040341-08$06.00

nado measurement problem (Smith and Holmes, 1961) was a long-wavelength analogy to our Doppler lidar application to waterspouts. As a preliminary to this study, the Doppler lidar technique was tested on dust devils (Schwiesow and Cupp, 1976). This dust devil experiment quantitatively confirmed the existence of subvortices reported by Sinclair (1973), and revealed peak wind speeds of 22 m s^{-1} from a sample of 43 dust devils.

2. Experimental procedures

The instrumentation and measurement process has an important bearing on interpreting the velocity spectra. In this article we describe the characteristics of Doppler lidar because the technique is not yet widely applied to measuring microscale atmospheric phenomena and because it gives a different type of information than point-sample wind sensors.

Familiarity with Doppler weather radar (Doviak *et al.*, 1979) will help the reader understand Doppler lidar. Although the size of the sample volume with typical radars is orders of magnitude larger than that for the lidar used in this experiment, many concepts from Doppler radar, such as Doppler spectra and volume integration, carry over into Doppler lidar. Doppler radars have not been applied to the waterspout question, but large groundbased radars have collected data from severe storms that contained tornadoes. Mesoscale cyclones associated with a tornado are on a scale appropriate to the measurement capability of a pulsed Doppler radar.

a. Technique

Doppler lidar measures the velocity component along the optical line-of-sight of scattering particles in the remote focal region of the optical system. The focal region is the volume of the atmosphere where the radiation from the laser transmitter is focused to the maximum possible flux density and from which particle-scattered signal can be detected efficiently. Fig. 1 gives an indication of the relationship between focal region, waterspout, aircraft, and sea surface. Scattering from regions outside the focal volume makes a negligible contribution to the signal, and focusing is required to obtain a large enough signal intensity to do Doppler processing of the return. Details on the size of the focal region and its dependence on system parameters are discussed in Schwiesow and Cupp (1980). A backscatter geometry, in which the scattered radiation is collected at 180° from the direction of the incident radiation, is the most practical for a mobile system because a single aperture can be used for both the transmitter and receiver. An aircraft as a lidar platform provides the necessary mobility for successful waterspout interceptions.

The velocity measurement is made by comparing the frequencies of optical radiation (in this case in the infrared near 10.59 μm wavelength or 28.31 THz) backscattered from atmospheric targets to the transmitted frequency. If the scattering targets are in motion, the scattered radiation will be Doppler shifted in frequency. With a backscatter geometry, only the velocity component along the lidar line of sight will cause a detectable Doppler shift. A shift of 188.9 kHz corresponds to a velocity component of 1 m s^{-1}. The calibration constant between frequency shift and velocity is simply 2 divided by the wavelength of the laser; thus the velocity is known to the same accuracy as the measurement of Doppler frequency shift.

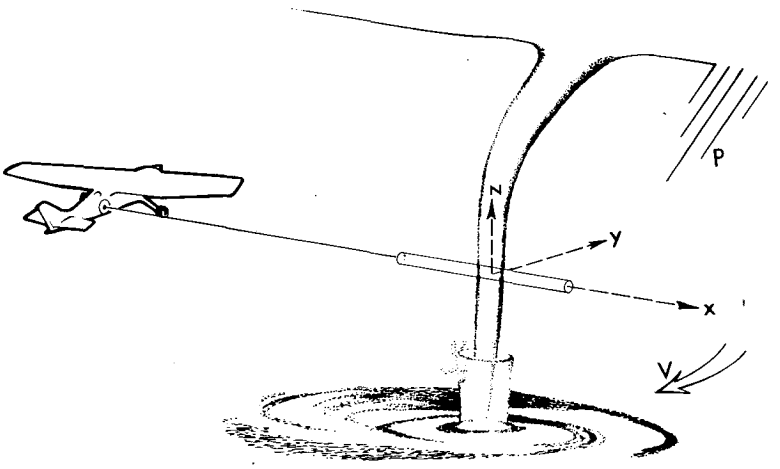

FIG. 1. Lidar waterspout sensing geometry. Main core of storm and precipitation is at P. Cold outflow V moves waterspout (in updraft region) away from storm core. Flight path is parallel to y. Lidar senses the absolute value of velocity component parallel to x. Sensing volume is parallel to x, centered at $x = 0$, and moves in the y direction.

To measure the frequency shift, we used optical heterodyning, which mixes the returned signal with a planewave local oscillator on a non-linear detector. Optical heterodyning requires signal phase fronts that match the local oscillator, so only scattered signal from the diffraction-limited focal volume of the lidar optics is detected efficiently. Lidar sensitivity to scattering particles falls off rapidly outside the focal region. The diameter of the velocity sensing region increases linearly with range, and the length of the region increases with the square of the range. This range dependence is directly analogous to the variation in scene size and depth of field with range for an image-forming optical system.

Either naturally occurring aerosols or cloud droplets serve as flow tracers for a lidar. The sensitivity of the 10.6 μm infrared lidar to particles with radii smaller than ~ 1 μm decreases as the sixth power of the radius, and typical natural aerosol number densities decrease very rapidly for particle radii above 1 μm. As a result, the lidar was most strongly affected by natural aerosol particles in the 1–3 μm radius range, except where cloud droplets occurred and provided a locally large number of large particles. In practice we found that waterspout condensation funnels that were visible to an observer had a sufficient number of cloud droplets to produce a strong lidar signal for our system, and that it could detect easily vortex data only from those regions marked by cloud particles.

To investigate how well cloud droplets follow the flow, we note that the median diameter of the droplets formed by pressure drop in the vortex must be no larger than that for a continental cumulus, or 10 μm (Fletcher, 1969). The terminal velocity of such particles for 1 g acceleration is 3×10^{-2} m s^{-1}, and the terminal velocity is directly proportional to the acceleration, in the Stokes region (Dennis, 1976). The greatest change in tangential (circumferential) velocity around a waterspout we observed was 10 m s^{-1} in half of a revolution of a vortex with 12 m radius and 20 m s^{-1} average tangential velocity. This represents an acceleration of less than 0.6 g or a difference of less than 2×10^{-2} m s^{-1} between the tangential velocity of the fluid and the cloud droplet flow markers. Tangential velocity in the vortex is the most important variable measured by the lidar. Radial (centripetal) accelerations are larger. In the largest-acceleration case observed, a tangential velocity of 26 m s^{-1} at a 5 m radius, the radial acceleration was ~ 14 g which leads to a difference between flow and particle velocity of up to 0.4 m s^{-1}.

b. *Velocity spectra*

Within the focal volume there will be many scattering particles (e.g., 10^6–10^8 m^{-3} for aerosols and dense cumulus) with a distribution of velocity components toward or away from the lidar. Because of the complex distribution of velocities, it is not possible in most cases to characterize the line-of-sight airflow component in the sample volume by a single value as is often done with Doppler data. A useful way of presenting the data is to plot the intensity of backscatter for each velocity. This produces a backscatter-weighted distribution of number of particles with a given velocity versus velocity (a velocity spectrum).

From a velocity spectrum it is possible to estimate the highest speed component present that is represented by a sufficient number of scatterers to produce a received radiant power greater than the system noise level. The most probable velocity (peak of the spectrum), average velocity (first moment of the spectrum), and sub-resolution-volume-scale turbulence (second moment of the spectrum or approximately the spectrum width at the -3 dB points) are also available from the spectrum. Complex spectral features, such as multiple-peaked spectra, require interpretation in terms of the waterspout geometry and sensing volume orientation.

Because the data are measured and recorded as a series of velocity-component spectra, this format is the most basic representation of the data.

c. *Lidar hardware*

The cw infrared Doppler lidar system used for the demonstration of waterspout velocity measurements incorporates a CO_2 laser transmitter, which produces a radiant flux of 2.7 W at 60 m range. We used the same telescope for transmitting and receiving with a polarization beamswitch for isolation. The 30-cm aperture telescope serving as a transceiver produces a sensing volume in the shape of an elongated cylinder, aligned with its axis along the lidar line of sight, with dimensions depending on range. The focal volume is approximately a cylinder 2 cm in diameter by 12 m long if centered at a range (focus) of 100 m. At a range of 500 m, the sensing region is approximately 10 cm in diameter and 300 m long.

For optical heterodyne mixing and detection we used a liquid-nitrogen-cooled HgCdTe photoconductor. Some of the transmitter output was used as the local oscillator (homodyne operation) so that, in the absence of Doppler shift on the returned signal, the radiofrequency output of the detector would be at 0 Hz. Velocities toward or away from the lidar both result in positive frequency differences (beat frequencies) that are indistinguishable from each other if the magnitudes of the line-of-sight components are the same. In other words, the lidar determines only the magnitude and not the sign of the longitudinal component of the velocity. This limitation was not a serious problem for waterspout observations.

A scanning spectrum analyzer produced a com-

plete velocity spectrum in 10 ms or 20 ms, depending on the setup, with 4–6 ms dead time between scans. We recorded the spectra on analog magnetic tape along with a time code for identification. At the same time that the spectra were taken, we took high-speed motion pictures of the waterspouts at 54 frames per second with an overlaid time code for identification. The movie camera, with a 60 mm lens and super-8 color film, was boresighted so that the lidar sensing volume was at the center of the field and marked with an overlaid circle.

The velocity resolution was ~1% of full scale on the spectrum analyzer output. A velocity accuracy of ±3 cm s^{-1} was set by the uncertainty in laser linewidth. Both these values are much less than uncertainty from the turbulence width of the spectra and may be neglected. Although the lidar frequency response allows velocity measurement to 250 m s^{-1}, most data were taken at 25 and 50 m s^{-1} full scale settings.

The overall lidar system required 750 W of 115 V ac power and weighed 175 kg. A scanning mirror covered ±15° in azimuth and elevation.

d. Platform

If we use sighting data from the Key West, Florida, National Weather Service office, an assumed sighting range of 17 km, and a lidar operating range of 1 km from roads, it is possible to calculate an upper limit estimate of 2% probability that a groundbased lidar would be able to obtain useful waterspout data in a 30-day experiment. A 30-day intercept probability estimate of 1% for a groundbased system results if the sighting frequency from aircraft is adjusted for the comparative area coverage and mobility of a groundbased unit. The obvious conclusion, based on these probabilities as well as practical experience, is that an airborne lidar is necessary to have a greater than 2% chance of obtaining waterspout velocity data in a 30-day experiment.

The Doppler lidar was mounted on the starboard side of a single-engine, STOL-modified Cessna TC-207 aircraft. Inflight test experience demonstrated that the best waterspout scanning technique was to fly by the vortex with the aircraft in straight and level flight. Manual scanning of the funnel was not a useful technique because the vortex was within range for less than 5 s. With the lidar axis perpendicular to the flight path, aircraft translation sweeps the lidar sensing volume through the waterspout. Any effect from aircraft velocity was minimized by adjusting the azimuth angle so that the lidar-observed airspeed component was 0 ± 0.5 m s^{-1}. This was necessary because a constant airspeed component added to the vortex velocity, which changes sign on either side of the axis, would introduce an artificial asymmetry in the waterspout velocity observations. Average ground winds with components transverse to the flight path are not observed by the lidar because the aircraft follows the mean transverse wind. Fluctuations about the mean can be observed by the lidar.

For a fixed lidar azimuth, the total time to scan a waterspout was less than 1 s. During this time the roll and yaw of the aircraft were small even in rough air. From the known aircraft speed and spectrum measurement rate the diameter of the infrared scattering part of the waterspout can be unambiguously determined (independent of range) if the aircraft is in straight and level flight. The aircraft true air speed (corrected for static error resulting from the open viewing port) on the waterspout passes was 54.3 m s^{-1} ± 8%. The aircraft yaw rate from the boresighted motion pictures was less than 3×10^{-3} rad s^{-1} except for isolated, roll-coupled impulses, which did not occur during any waterspout scans. Turning introduces an uncertainty of ±3% in the effective air speed of the sample volume at 500 m range. When a ±2% uncertainty in data rate is included, the overall uncertainty in waterspout radius as sensed by the lidar backscatter criterion is the greater of ±13% or the 0.75 to 1.4 m distance between data scans. Distance between scans is the product of the 14 ms or 26 ms spectrum repetition period and the true air speed. Comparison of photographic and lidar data gives the result that the lidar return diameter and visual diameter are the same to within the uncertainty given by the interscan and interframe periods.

Passes were made at altitudes ranging from 68 ± 8 m above the surface (the minimum safe altitude for near-storm conditions) to cloudbase at approximately 600 m. The most successful elevation angle for scanning was zero (horizontal). Occasional passes near cloud base were made with an elevation of +6° to scan the visible funnel when the condensation did not reach down to flight level. For low passes, 0° elevation was used. Attempts to scan below the minimum altitude of 68 m by using negative elevation angles were not successful because the variable roll angle of the aircraft and the difficulty of estimating range caused the sensing volume to intersect the sea surface at locations other than at the waterspout spray ring.

Estimating range to the waterspout before the pass in order to set the lidar focus was a difficult experimental problem. Because the sea surface is essentially featureless and the visible funnel diameter neither known nor the same for different waterspouts, visual range cues were inadequate. During the pass the visually observed angular speed of the spout gave a range cue that was too late to be of use in setting the focus. A range setting of approximately 500 m gave the best probability of useful

data. At ranges less than 500 m, the range gate (focal depth) is less than ±150 m and the chance of missing the waterspout by incorrectly estimating the range increases as the range decreases. The effect of improper focus is a reduction in signal to noise so that the velocity spectra cannot be detected. The received signal per scatterer decreases with the square of the range increase so that even if the chance of having the vortex in the resolution volume is large for ranges greater than 500 m, the signal level for typical cloud particle densities was too small to be useful. The product of signal strength times intercept probability as a function of range has a broad peak at 500 m for the lidar system used.

e. Backscatter coefficient and structure resolution

Although the azimuthal resolution (spot size) of the static lidar was ±10 cm at 500 m range, data were taken every 0.75 m along the aircraft flight path in the rapid spectrum repetition mode. The value 0.75 m is the effective spatial resolution of the data. This resolution was adequate to resolve the structure of the waterspout as a function of distance from the vortex axis in the y-z plane. We consider coordinates with x parallel to the lidar line of sight, z vertically upward, y parallel to the flight path, and the y-z plane containing the vortex axis as sketched in Fig. 1. In contrast, there is essentially no resolution in range (along x) through the funnel. The velocity spectrum at any y was the range-integrated (over x) value, consisting of velocity contributions from all particles in the sensing volume. Each scattering particle contributed to the spectrum in proportion to its backscatter coefficient, giving a power density distribution as a function of velocity.

The observed velocity spectra are the backscatter-weighted line-of-sight velocities in the remotely sensed region of the atmosphere. Signal from ambient aerosols appeared near zero frequency because the relative motion between the aircraft and the ambient aerosols (airspeed) had a near-zero x component. Signal at nonzero x velocities appeared only when the beam intersected the vortex condensation funnel because (1) the backscatter was large from the cloud droplets, and (2) the vortex introduced nonzero x velocity components. Both conditions were necessary to observe a Doppler lidar spectrum from the waterspout. The sudden onset of signal occurred at $y = -r_c$ where r_c is the radius of the condensation funnel of the waterspout.

A small atmospheric vortex must have sufficient condensation to be visible in order to be clearly detected by the infrared Doppler lidar system used in this experiment. Except when operating in areas that had been precipitation-scavenged within the previous 15 min, the lidar could detect clear air (ambient aerosol) returns from the atmosphere with a 3–5 dB signal-to-noise ratio on the raw spectral data in a 10-ms scan with no time averaging. However, the ambient aerosol fills the entire sampling volume whereas a 10-m diameter clear vortex fills only a small fraction of the sensing region and is therefore not detected. Typical signal return levels from condensation funnels were ~15 dB above the noise.

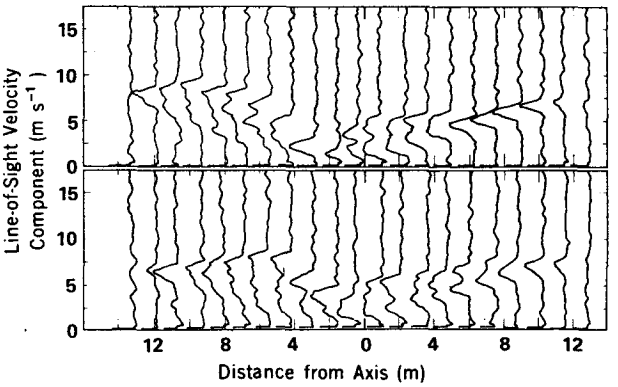

FIG. 2. Composite of velocity spectra for two flybys of a double-walled waterspout. Departures from a straight vertical line are relative backscattered power at the velocity indicated on the ordinate. The two data passes in upper and lower parts of the figure were taken approximately 3 min apart.

3. Results

The experiment demonstrated the feasibility of using airborne Doppler lidar to make one-component measurements of waterspout velocity.

As an example of the type of data available from this instrumentation, we show measurements of a single waterspout in Fig. 2. This waterspout was of double-wall structure (based on the visual data), which has the appearance of two concentric cylindrical shells. Golden (1974) mentioned this type of structure. Data were taken on 26 August 1976 approximately 15 km north of Key West, Florida.

a. Velocity spectra

Fig. 2 shows two series of waterspout velocity spectra taken approximately 3 min apart as successive passes of a single waterspout. The condensation funnel extended 100 ± 30 m below cloudbase for this example; data were taken just above the bottom of the funnel. Time increases from right to left in Fig. 2. Spectra start at the right at $y = -r_c$ (as in the geometry of Fig. 1 where r_c is the radius of the condensation funnel) and progress through the funnel to $y = r_c$. The abscissa is the distance from the vortex axis. Each spectra (the false third dimension in Fig. 2) represents the backscatter from all particles, integrated along x through the lidar sensing volume, that had an x component of velocity within the bandpass of the spectrum analyzer centered at

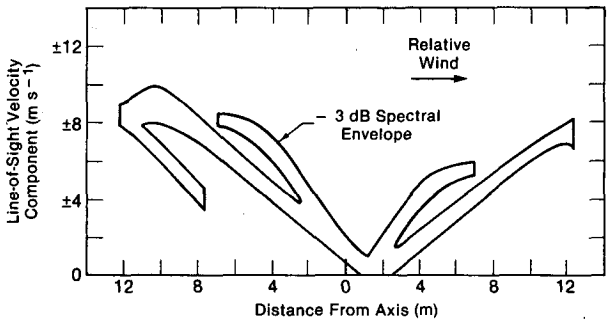

FIG. 3. The −3 dB spectral power contour from the upper composite in Fig. 2. Predominant backscatter-power-weighted velocity component at any radius is between the contour lines. This figure shows that the maximum observed line-of-sight component of the velocity is near the outer edges of the condensation funnel, although the velocity outside the condensation region could not be observed by the lidar used in this experiment. A striking feature is the double-valued velocity indicated at radii ≤ 7 m. The double peak in the velocity spectra corresponded to a visual double wall in the waterspout. Note the increased turbulence (velocity difference between upper and lower contour lines) on the upwind side of the waterspout and the asymmetry.

the velocity (optical difference frequency) given by the ordinate in Fig. 2.

Some characteristics of Doppler lidar measurements of waterspouts can be observed in Fig. 2. The sudden appearance in the lower set of traces (first pass) of a backscatter signal between $y = -13$ and -11.5 m and the disappearance between $y = 12$ and 13.2 m are evident. This indicates a radius of the infrared-backscatter-detected condensation funnel of $r_c = 12.4 \pm 2.0$ m. The spectra show a smooth transition from trace to trace, except for the sudden appearance of a second component in the spectra at a scan position of ~7 m.

In the three minutes between the first (lower) and second (upper) pass, the general features of the vortex remained qualitatively the same. The inner condensation funnel contracted and the maximum velocities increased. The persistence of the two peaks in the backscatter-power-weighted velocity distribution shows both from trace to trace (consistent in space) and from pass to pass (consistent in time).

b. *Velocity structure*

A simplification of the velocity spectra composite of Fig. 2 allows one to interpret some aspects of the velocity structure. In order to produce the spectral contours of Fig. 3, the −3 dB points on each spectrum in the upper half of Fig. 2 were plotted as a function of distance from the vortex axis. These points were connected by smooth curves to produce the −3 dB contour in Fig. 3. The sign of the line-of-sight velocity component must be opposite on opposite sides of the vortex axis so that reflecting one branch (side) of the −3 dB contour about the zero velocity axis clarifies the contour shape near $y = 0$, where the spectra were changing rapidly. Fig. 3 shows both branches (the right and left portions corresponding to advancing and retreating sides of the waterspout) of the spectral contour on the same side of the abscissa to emphasize that the Doppler lidar used for this feasibility demonstration did not determine the sign of the velocity component along the x axis.

The possibility of relative motion along the line-of-sight direction between the lidar and the vortex axis means that the $y = 0$ point (geometric midpoint or zero radius) of the −3 dB contour (vortex axis) need not have a zero line-of-sight velocity component. Fig. 3 shows that the midpoint of the condensation funnel and the zero-velocity y coordinate did not coincide in this case.

The velocity value at the middle of the contour at $y = 0$ (zero radius) indicates that the relative motion between the lidar and vortex axis was ~1.3 m s^{-1} along the line of sight. From the geometry of Fig. 1, the waterspout was moving toward the lidar; the Doppler lidar as used in this demonstration experiment could not determine the sense of the motion. With motion toward the lidar and the fact that time and y-direction scan increase from right to left in Fig. 3, it is evident that the waterspout was cyclonic.

The velocity structure of the waterspout showed a distinct asymmetry with respect to the storm outflow. The cold outflow associated with the convective cell flows past the vortex and tends to move the base of the waterspout away from the storm center (Golden, 1974) as indicated in Fig. 1. The outflow for the case given in Fig. 3 had a $-y$ component (from the front starboard quarter), so that the left branch of the velocity contour diagram represents the windward side of the vortex; the right branch is the lee side. Because the flow field at the location of the vortex moves past the vortex (local wind speed greater than vortex translational speed) the strongest interaction between the outflow and vortex was on the windward side. The strong turbulence associated with the interaction between the vortex and the outflow caused the larger spectral width at the peak of the left branch. Strong turbulent mixing distorts the tangential flow on the windward side of the vortex. A slight spectral broadening (increase in turbulence) existed at the lee edge of the funnel where we might expect more shear than in the interior of the waterspout.

The appearance of a second velocity value for radii $r \leq 7$ m is a striking feature of Fig. 3. This inner-radius velocity structure corresponded to a visual double funnel. The inner funnel had a velocity to distance correspondence different from the outer funnel. We assume from the data a dynamic difference between the two components of the vortex system, but further analysis and modeling are required to clarify the structure.

The data show a third velocity value for 7.5 m $\leq y \leq$ 11 m. This data could correspond to a shell that is more slowly rotating than other parts of the waterspout. This outer scattering layer, whatever its origin, existed only on the upwind side of the funnel and was not present in the visual data. One hypothesis is that this feature occurred when moist outflow from the storm achieved some rotational component and experienced sufficient pressure drop for slight condensation to occur. With increased mixing as the ambient flow moved past the vortex the condensation became less and the droplet density was no longer large enough to give a measurable lidar return. In the absence of data on a third (lower) velocity value on the lee side of the vortex, it is impossible to conclude that the outer structure represented a closed, circularly cylindrical shell, although it may have been such a flow.

The velocity difference between right and left branches of the inner core in Fig. 3 is approximately 2.6 m s^{-1}, which is just twice the on-axis translation of 1.3 m s^{-1}. Near zero velocity, the slopes of right and left sides of both vortex shells are identical. The maximum velocity on the right side is 8.3 m s^{-1}. The intercept of the left side initial slope with the outer radius of the funnel (r = 12.4 m) is 10.9 m s^{-1}. The right to left difference between projections is again 2.6 m s^{-1} or twice the translation velocity. If we correct for translation, the peak tangential velocity, including turbulence, was 9.6 m s^{-1} for this sample case. Alternatively, we can use the slope of the velocity dependence to calculate a peak angular velocity of 1.5 rad s^{-1} for the inner shell and 0.75 rad s^{-1} for the outer. The velocity deficit at the upwind edge of the funnel is 2.1 m s^{-1}, which is the difference between the projected value of 10.9 m s^{-1} and the actual observation of 8.8 m s^{-1} at the edge. It is reasonable to relate the velocity deficit to mixing between the vortex and more slowly-rotating ambient flow. Because of this mixing, the tangential speed was not the same all around the funnel, but the data indicate that the distance from the axis to the edge of the funnel (infrared scattering funnel radius, r_c) was the same on both sides (right and left) of the vortex. The equivalence of r_c on both sides was established from the axis as determined by symmetry of the velocity structure near the core and the lidar-sensed outer edges of the funnel.

c. *Comparison with aircraft penetration data*

The lidar data are complementary to the gust-probe horizontal wind data of Leverson *et al.* (1977). The lidar gave much more detailed wind data in the funnel than the gust probe, but the aircraft data measured the tangential flow as far as 200 m from the vortex core.

The translation-corrected maximum velocity measured in the single lidar instrumentation example was 9.6 m s^{-1} in the part of the waterspout marked by cloud droplets. Other waterspouts may show a larger maximum velocity. Values from Leverson *et al.* (1977) ranged up to a maximum of 28 m s^{-1} on the back side of the spout but to only 13.1 m s^{-1} on the front (initial penetration) side. The consistent asymmetric horizontal velocities for both cyclonic and anticyclonic waterspouts were attributed to the neglect of yaw accelerations of the aircraft during penetrations, so the back side velocity values may require substantial correction. Golden (1974) gave a conservative estimate of 27 m s^{-1} for the photogrammetrically-derived mean tangential speed in the outer wall of one waterspout.

One major advantage of the lidar remote sensing technique is that the measurements are independent of vortex-induced effects on the aircraft such as yaw acceleration. On the other hand, penetration flights measure temperature, pressure, and vertical velocity in addition to horizontal wind speed.

d. *Comparison with other remote sensing techniques*

There are a number of improvements in the instrumentation that was tested which would improve its ability to obtain useful waterspout data. Introduction of a frequency-offset local oscillator (Schwiesow and Cupp, 1981) would distinguish between positive and negative line-of-sight velocity components because zero velocity would correspond to a chosen frequency difference between transmitter and local oscillator.

The problem of estimating range and setting focus, discussed in Section 2, could be addressed by rapid scanning in range during a pass. Only those focus positions giving sufficient signal to noise could be analyzed. This type of operation would require much more rapid scanning of the Doppler spectrum and a higher duty cycle than was available in the scanning spectrum analyzer used for our experiment. Although spectrum analyzers based on a surface acoustic wave dispersive delay line offer faster scan and a higher duty cycle, presently available units do not have the frequency range for waterspout work at 10.6 μm. From a signal utilization point of view, signal wasted by a fixed-focus, frequency-scanning system such as used in this experiment would be approximately equivalent to signal wasted by a scanning-focus, frequency-parallel analysis scheme. A pulsed infrared Doppler lidar that operates with an average transmitter power and telescope aperture similar to the one described in this paper could possibly be useful if the Doppler processing were efficient enough to obtain good signal-to-noise from a collimated (infinity-focus) optical system at ranges short enough for good pointing accuracy. Neither the lidar hardware nor the processing system for such an approach has been demonstrated in a package that is suitable for

mounting in a light aircraft, so the applicability of the pulsed approach to the range estimation problem cannot be determined.

There appears to be no practical way of increasing the spatial resolution of an infrared Doppler lidar along the line of sight. A larger telescope aperture for reduced depth of field is not practical in a light, airborne system, and atmospheric refractive index inhomogeneities limit the size of the coherent effective aperture of a telescope. An increase in range resolution by pulsing is not possible, because the frequency broadening from a 300 ns pulse, for example, giving 50 m range resolution would cause more than 15 m s^{-1} uncertainty (broadening) in the velocity spectrum. In addition, the data processing for a range-resolved return is difficult and a 50 m range resolution is completely inadequate to resolve any waterspout structure in the line-of-sight direction. The limit on the product of range and velocity resolution for a pulsed lidar is different than the limit in the radar case, because for radar it is possible to track the relative phase between local oscillator and signal from pulse to pulse. This phase coherence between pulses is not yet available in the infrared.

There are a number of parallels between Doppler radar (Doviak *et al.*, 1979) and lidar. The radar analogue of our cw infrared Doppler lidar should be useful for waterspout studies. Although the resolution in azimuth of a radar with a practical antenna size is not as good as the lidar, it should be adequate at a 500 m range. A data analysis similar to that presented here may be applicable. Airborne pulsed Doppler radars typically require a large aircraft for mobility. The range capability of such radars is far greater than our lidar, but it is difficult to achieve a resolution transverse to the beam of less than 1 m. Detection of signal from 10-μm diameter cloud droplets requires a short wavelength (e.g., 8 mm) radar, but research on the application of such systems is not complete enough to evaluate the practicality of a light, airborne system for waterspout research.

4. Summary and recommendations

The experiment with an airborne Doppler lidar demonstrated the ability of this type of instrumentation to provide data on the velocity structure of waterspouts. Measurements do not interfere with the vortex. They provide resolution in azimuth that shows detail down to a scale of ~0.75 m across the funnel for the instrumentation we used.

Because the lidar we used integrates velocity contributions along the lidar axis within the resolution volume, there is no useful resolution in the line-of-sight direction and care must be exercised in interpreting the velocity spectra. No data were available with the lidar system used in this experiment from parts of the waterspout not marked by visible condensation or spray.

Data for the vortex used as an example of instrument capabilities revealed a two-peak velocity structure corresponding to the visually observed double-walled funnel. Interaction between the vortex and the storm outflow moving past it caused a slowing of tangential speed and increased turbulence on the upwind side of the waterspout compared with the lee side.

For future work we recommend that data be taken lower in the spray ring and inflow region of the waterspout. Safety at very low altitudes combined with mobility would probably require the use of a seaplane as a lidar platform. Lidar instrumentation to measure the vertical velocity structure in waterspouts would add to our knowledge of waterspout dynamics. Such lidars are being developed (Lading *et al.*, 1978; Schwiesow *et al.*, 1977) but have not yet been applied to vortex measurements or used with an airborne platform.

Acknowledgments. This work was supported in part by the U.S. Nuclear Regulatory Commission under Interagency Agreement RES-76-106 NRC, FIN B5691 with NOAA. The enthusiasm of W. N. Hess was instrumental in beginning the waterspout study; the contributions of J. H. Golden are gratefully acknowledged.

REFERENCES

Dennis, R., Ed., 1976: *Handbook on Aerosols*. Energy Research and Development Administration, p. 122 [NTIS TID-26608].

Doviak, R. J., D. S. Zrnić and D. S. Sirmans, 1979: Doppler weather radar. *Proc. IEEE*, **67**, 1522–1553.

Fletcher, N. H., 1969: *The Physics of Rainclouds*. Cambridge University Press, p. 115.

Golden, J. H., 1974: The life cycle of Florida Keys' waterspouts I. *J. Appl. Meteor.*, **13**, 678–692.

Lading, L., A. Skov Jensen, C. Fog and H. Andersen, 1978: Time-of-flight laser anemometer for velocity measurements in the atmosphere. *Appl. Opt.*, **17**, 1486–1488.

Leverson, V. H., P. C. Sinclair and J. H. Golden, 1977: Waterspout wind, temperature and pressure structure deduced from aircraft measurements. *Mon. Wea. Rev.*, **105**, 725–733.

Schwiesow, R. L., and R. E. Cupp, 1976: Remote Doppler velocity measurements of atmospheric dust devil vortices. *Appl. Opt.*, **15**, 1–2.

——, R. E. Cupp, M. J. Post and R. F. Calfee, 1977: Coherent differential Doppler measurements of transverse velocity at a remote point. *Appl. Opt.*, **16**, 1145–1150.

——, and R. E. Cupp, 1980: Calibration of a cw infrared Doppler lidar. *Appl. Opt.*, **19**, 3168–3172.

——, and ——, 1981: Offset local oscillator for cw laser Doppler anemometry. *Appl. Opt.*, **20**, 579–582.

Sinclair, P. C., 1973: The lower structure of dust devils. *J. Atmos. Sci.*, **30**, 1599–1619.

Smith, R. L., and D. W. Holmes, 1961: Use of Doppler radar in meteorological observations. *Mon. Wea. Rev.*, **89**, 1–7.